Automatic Laser Cavity Adjustment and Beam Profiler System

William Bowman, AJ DeSantis, Bryce Moon, and Nicholas Pinkham

College of Engineering and Computer Science, College of Optics and Photonics, University of Central Florida, Orlando, Florida, 328166-2450

***Abstract* — The objective of this project is to design and implement a freely attachable, automated adjustment system for the output coupler of an open cavity laser. The system will adjust the couplers tilt knobs until the cavity lases, reducing the time and effort needed for setting up experiments and applications which make use of open cavity lasers. The project will also include a beam profiler running simultaneously to the adjustment system, enabling real time analysis of the beams development, while also outputting relevant beam parameters, such as beam waist and divergence.**

***Index Terms* — Automation, Laser Beams, Laser Cavity Resonators, Lasers and Electro-Optics, Laser Excitation**

I. Introduction

The motivation for this project is derived from the time and effort it can take to achieve a lasing condition with an open-cavity laser. Above the lasing threshold condition, a laser's output is dominated by stimulated emission as opposed to spontaneous emission, the spectral linewidth drastically decreases, and the slope of the relationship between input power and output power is orders of magnitude greater than in the non-lasing condition. In general, a laser that is lasing produces much greater power than one that is not lasing. An important element in achieving the lasing condition is properly adjusting the couplers (mirrors) which are located on either end of the cavity. One of these is fully reflective, and is usually fastened, even for open cavity lasers. The other coupler is only partially reflective, allowing the laser to output through it, and tends to be free standing, allowing for manual adjustment. This leads to the partially reflective mirror being referred to as the output coupler. Making the adjustments necessary for lasing by hand can often be tedious and frustrating, as the process consists essentially of changing the pitch and angle of the mirrors by twisting knobs on the mirror mounts. The scale of these adjustments becomes exceptionally minute as the lasing condition is approached, and one small mistake can cause major setbacks in progress. This project automates this process, removing the need to manually adjust the lasing system and ameliorating any related stress.

This automation is accomplished using a custom power meter, which, in conjunction with 3-D printed housings, can interface with an open cavity laser's output coupler. These housings have been designed for near-universal applications to different couplers, and simply fit over the adjustment knobs of a coupler. Physical movement of the knobs is governed by continuous motors, while a servo motor offers enhanced control of the coupler's angular orientation.

Furthermore, our system can perform a qualitative analysis on the laser beam. This is necessary for the second stage of what the system is able to accomplish. Once the laser has been brought to the lasing condition, the system seeks to maximize output power and mode quality via the power meter and qualitative beam analysis. Through this beam analysis process, elements of the beam, such as beam waist, divergence angle, and mode quality are observed and communicated to the user. In addition, a live feed of the beam's intensity profile is presented to the user. The aforementioned factors are all important when deciding what beams to use for differing applications and determining whether the beam displays any negative characteristics like astigmatism, jitter, etc.

The issue of manually adjusting an optical system is something that we have frequently encountered, personally by working in the lab and through the complaints of other students and even professors. Thus, we believe that this aspect of the project reaches a niche but certainly existing market, mainly focused within the academic community, for both research, development, and teaching applications. The beam profiler broadens the potential market for our system to industry use, while still holding relevance to the aforementioned academic fields. This is especially applicable in the manufacturing of closed cavity lasers, in which both couplers are hard fastened to the cavity. These lasers must be verified to have the highest output power and mode quality possible before permanently aligning the couplers. Automating this alignment process significantly reduces the potential for human error.

II. SAFETY STANDARDS

To ensure the health and wellness of our team members, we adhered to both electrical and laser safety standards during the duration of the project. The laser standards are set forth by ANSI Z136.1 – Safe Use of Lasers while electrical standards are from IEEE C95.1-2019.

III. SUB-SYSTEM ANALYSIS

We have divided the main body of this paper into three sections, each focusing on a different aspect of the combined system. As the beam profiler is the most isolated subsystem within the scope of the project, this will be discussed first, followed by in depth analysis of the power meter, motors, and their respective housings, which are all heavily interconnected. The paper ends with a discussion of the PCB design and laser alignment software.

A. Beam Profiler

From a hardware perspective, the beam profiler is likely the simplest sub-system of the overall project, consisting primarily of Raspberry Pi 4 microcomputer and a connected Raspberry Pi HQ camera. The RP equipment was chosen due to its low cost, high performance, and preponderance of freely available guides, projects, and forums relating to the hardware. The camera itself has excellent performance across the board, meeting or surpassing similarly priced camera benchmarks of resolution, sensor size, frame rate, etc. The sensor size in particular was an important factor to consider, as we want the system to be able to accurately profile a large array of different lasers, with differing spot sizes. The decision on which camera and microcomputer to purchase was made simpler by the fact the RP HQ camera interfaces exclusively with other RP products, forcing our hand in the selection of the beam profiler components.

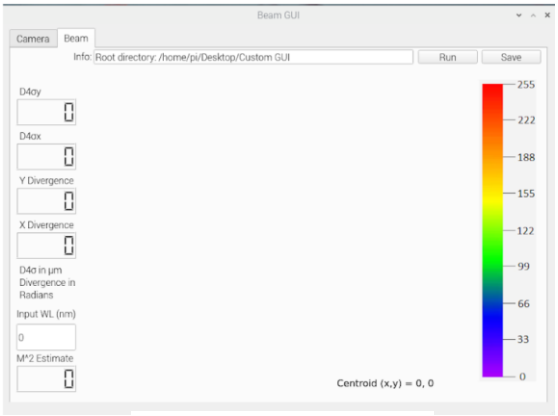

Figure 2, Beam Profiler GUI

Beyond these two electronic elements, the profiler also makes use of a neutral density filter, reducing the likelihood for sensor damage on the camera from a high intensity laser, and a focusing optic, needed for calculating the beams divergence (to be discussed more in-depth later). Although mechanically simple, this was counterbalanced by the computational complexity required of the system. In order to effectively communicate information relevant to the beam and to provide a live visualization of the beam profile, a custom graphical user interface (GUI) was needed. This was done using the PyQT5 library, which enabled the creation of a main GUI window, wherein other widgets, such as text boxes, controllable digit displays, user input areas, camera feeds, and buttons could be placed. Using this library, a large number of initialization, analysis, and communicatory elements are included in the GUI. The final design of the GUI is shown below, as well as an example of the GUI running with an impingent beam.

As shown in the above images, one aspect of the GUI is the ability to switch between viewing tabs of the beam. The first tab, labeled ‘Camera’, displays the raw, unprocessed feed from the camera. This feed shows the true color of the

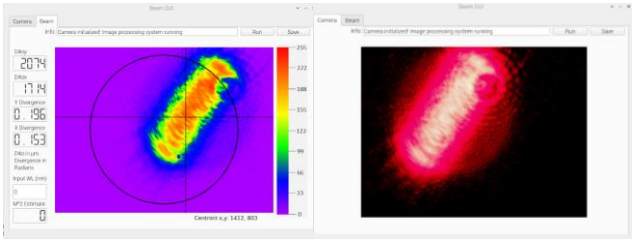

Figure 1, Beam Profiler in both 'Beam' and 'Camera'

beam and lacks any derived beam parameters or masks. The second tab, ‘Beam’ contains all these aforementioned features. Most prominent of these is a color mask, which when referenced with the color bar to the right of the camera feed, color codes the beam based off its intensity. A circular reticle mask is also applied to assist in centering the beam on the profile sensor. The final mask consists of two perpendicular bars which refresh constantly so that their intersection is located at the beam's centroid; if no beam is incident on the sensor, the centroid tracking masks auto-lock to the center of the image array.

When in the ‘Beam’ tab, a number of derived parameters are also shown on the left-hand side of the GUI. The first of these, the D4σx and y beam waists, are found using the computer vision (CV) library Image Moments Operator. Once the moments (M) are computed, the beam centroid $(\overline{x}, \overline{y})$ can then be found via equation (1). As seen in figures # and #, the centroid is displayed in the bottom right-hand corner of the GUI, below the camera feed. The centroid and the moments can then be combined in equation (2,3) to compute the D4σ beam waists. It should be noted that performing these operations will return values in terms of pixels, so to convert the waists into physical values, they pixel

quantities must be multiplied by the camera pixel size (1.55x1.55 μm for the RP HQ Camera).

$$\{\bar{x}, \bar{y}\} = \{\frac{M_{10}}{M_{00}}, \frac{M_{01}}{M_{00}}\} \quad (1)$$

$$D4\sigma x = 4\sqrt{\frac{M_{20}}{M_{00}} - \bar{x}^2} \quad (2)$$

$$D4\sigma y = 4\sqrt{\frac{M_{02}}{M_{00}} - \bar{y}^2} \quad (3)$$

Every other derived parameter within the GUI is based off these D4σ beam waists. The angular divergence, in radians, is approximated using the basic relationship in equation (4), in which a beam of waist size (W) can have its divergence found with the presence of a focusing lens. It must be kept in mind that divergences found via this equation are valid only if the image sensor is located at the focal length (f) of the optic, so system users should double check the distances between the Raspberry Pi camera and the focusing lens. With the beam waists and divergence, the GUI only needs one more parameter before it can solve for the M^2 estimate. The M^2 formulation, equation (5), input into the GUI requires the beams wavelength (λ), which can be user specified by typing it into the box located directly above the M^2 display box. If the wavelength input box is untouched by the user, the M^2 value returns 0.

$$\theta = \tan^{-1}(\frac{W}{f}) \quad (4)$$

$$M^2 = \frac{W \times \pi \times \theta}{4\lambda} \quad (5)$$

According to ISO standards, M^2 measurements must be predicated off multiple beam measurements near a focusing optic induced waist. Our system does not have a way to translate the profiler along the optical axis, meaning that the M^2 reading does not meet the ISO standard. Thus, we have labeled it as 'M^2 Estimate'. The baseplate upon which our optical elements are aligned, however, does allow for manual translation. A user of the system could make these translations, and with multiple profiler-computed beam waists, could then construct the beam fitting needed to obtain an ISO-standard M^2. The last major feature of the profiler is the 'Save' button. Once clicked by the user, a snapshot of the beam will be stored in a specified folder. The information within this snapshot includes 4 image files; The beams spatial raw spatial distribution, the beams color coded spatial distribution, the beams intensity distribution along the X-centroid, and the beams intensity distribution along the Y-centroid. In addition, there is a .csv file in which text containing the beam parameters is stored.

Because all other beam parameters are based off of the D4σ beam waists, ensuring the accuracy of the beam profilers waist measurements was key to giving valid values for all parameters. The mathematical derivations for the waists are valid and have been cross-checked with relevant literature, so testing just needed to ensure that the values being output by the profiler were reasonable and that there were no critical failures in the code or with the camera sensor. To perform this check, our team performed manual 1/e^2 beam waist measurements using the knife edge technique on a gaussian beam. Although D4σ and 1/e^2 waists will differ for shaped beams, for gaussian beams, they are identical, so our methodology was sound. 10 tests were performed, and the average percent difference between the computationally derived beam waist and the hand-measured waist came out to be ~3.4%. This percent difference is certainly due to inaccuracy of the manual measurement, as the computationally derived measurements are ideal. The similarity in values between the confirms the profiler returns legitimate beam waist measurements, which in turns makes the other profiler-calculated beam parameters valid.

When assessing the performance of the beam profiler as a whole, our group was pleased with the efficacy in which it visually communicated information on the beam and appreciated its functionality in saving a snapshot of the beam at any given time. Unfortunately, though, the memory of the Raspberry Pi proved to be detrimental to the profiler's functionality. While our group had initially hoped to purchase the 8-GB RAM model of the RP4, supply shortages forced us to into using the 2-GB RAM model. This downsize in memory is likely to blame for the main issue with the profiler, that being a dismal frame rate. Although highly variable, at times the frame rate could drop to 1 fps or freeze for seconds at a time. Although the profiler rarely crashes entirely, these slowdowns can impede a user's ability to observe as the beam develops with the adjustment of its output coupler. This poor framerate is a seemingly inescapable issue, even after downsizing the active area of the camera sensor and essentially simplifying the input. While the image could be further downsized to hopefully increase framerate, it has the negative drawback of reducing the beam spot size that can be accurately observed by the profiler.

B. Power Meter

The power meter subsystem performs two tasks within the overall device. The meter acts as a simple photodetector to detect whether the laser being used has achieved lasing and as a more proper power meter that enables the device to determine whether the laser is approaching maximum power or not.

Our range of laser wavelengths that our device can successfully function on is specified to be 400nm to 700nm. To accomplish such a detection range, we chose a silicon p-n junction photodiode as these are inexpensive and have the spectral range we desire. The specific photodiode that we chose was chosen for its desirable spectral response, relatively large active area, and inexpensive nature.

Since the cusp of the lasing region could have powers just barely above background noise, the reduction of background noise is important. Thus, the choice was made to operate the power meter in the photovoltaic mode due to the lack of dark current noise produced by the reverse bias that would be present in a photoconductive configuration. Another rationale for forgoing the photoconductive operation mode is the fact that the benefit of a high frequency response is not necessary for our application as we are not attempting to measure a rapidly modulating signal.

To aid in the noise reduction of the power meter, the photodiode was placed in a transimpedance amplifier circuit to keep the photodiode at a virtual zero volts. Potential noise is a major concern for the functionality of the coupler adjustment elements of the system, as high noise could potentially trigger a false lasing flag within the alignment software.

The load resistor of the power meter circuitry is used to ultimately determine the amount of light impinging on the photodiode. Ideally the circuitry would have multiple resistors that span a range of decades to be able to easily expand the device's usefulness. However, only one resistor may be read via the ADC ports of the Raspberry Pi Pico, providing a smaller range of workable laser powers. One could still operate the device with different laser powers but would have to go into the device and physically switch out the load resistor on the PCB for a load of differing ohmic resistance.

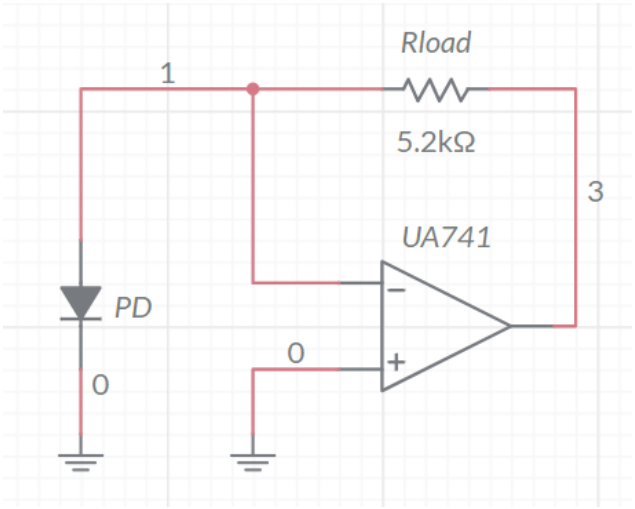

Figure 3, Photodiode with Transimpedance Amplifier Circuit

C. Mirror Mount Motors

In terms of what each sub-system does, the motor subsystem of the project is the only mechanical portion of the project and is the part responsible for adjusting the angle of the mirror and in turn changing the state of the light source. For hardware, the mirror mount motor system can be summarized as having seven key components, these are a battery pack, two dc-dc voltage converters, three servo motors, and a microcontroller. The mirror mount motor subsystem consists of three servo motors, two are the Fs90r rotational servo and the third is the DS3218 positional motor. All three motors are powered by a 6-volt battery pack consisting of 4 D-cell batteries, this is the same battery pack used as the voltage source for the power meter subsystem. Before reaching the servo motors, the battery back goes through two dc to dc stepdown voltage converters. The first voltage converter is dedicated to the two continuous while the second voltage converter is dedicated to the positional servo motor. These DC converters are used to keep the range of the voltage supplying the motor around 5 to 5.3 volts while also keeping the current constant. Lastly, the piece of hardware used to control the motors is the microcontroller known as the Raspberry Pi Pico, this device is also connected to the power-meter system and decides the movement of the servo motors based on the values read by the power meter.

Motor Name	DS3218	FS90R
Servo Type	Positional	Continuous
Weight	60 G	9 G
Torque (1) oz/in	263.8 @ 5 V	18 @ 4.8 V
Torque (2) oz/in	298.5 @ 6.8 V	21 @ 6 V
RPM (1)	93.75 @ 5 V	100 @ 4.8 V
RPM (2)	107 @ 6.8 V	130 @ 6 V

Table 1, motor specifications

For the designing of mirror mount motor system, there were two tasks needed to be performed by the motors, the first task is to adjust the angle of the mirror on the mirror mount by rotation the two knobs found on the mount; the second tasks that needs to be done is the swiveling of the mirror mount itself to check if the lasing state can be found with the current rotation of the mount knobs. For the task of rotating the mirror mount knobs, the FS90R continuous servo motors were selected due to motor's small dimensions as seen in figure # and only weighing 9 grams while being able to supply 18 oz. per in. as seen in table #. Having small dimensions allows the motor to be connected directly to the mirror stand without fear of blocking the laser while being light weight allows having to concern with the added weight affecting the positional motor's ability to rotate the mirror stand. Other benefits of the FS90R are that being a continuous servo the coding to control the direction is speed is rather simple, only needing to set a single value. Additionally, servo motors only need one pin from the Pico to control unlike a normal electric motor or a stepper motor which need two to four pins. For the stand motors there was a different set of requirements, the main two necessities being a higher torque to allow rotating of the mount stand and the ability to accurately control where the stand faces. The DS3218 was selected due to the 263 oz/in torque offered at 5 volts allowing it to adjust the stand with relative ease. Being a positional servo, our group is allowed to directly command where the DS3218 face.

D. Housings

One of the primary design challenges our group faced in developing this project was how to interface between the output coupler adjustment knobs and the motors themselves. While the coupler has only two knobs, one for vertical tilt and one for horizontal, our experience with manually achieving lasing had taught us that one of the best methods involved performing large rotations of the coupler itself, performing a sweep, in essence. To perform this type of sweep, we realized that we would need to be able to rotate the optical post upon which the coupler rests. The knob rotation was decided to be controlled by the continuous motors, while the post rotation would be dictated by the servo motor. For the adjustment knob interface, our group designed a ring-like holder with a notch separating the two ends, allowing the ring to bend and expand in order to fit around knobs of different sizes. A triangular protrusion was then created on the back face of the ring, which we affixed the continuous motors rotating propellor to. This design was then 3-D printed with plastic filament. The plastic offered very low friction with the metal of the adjustment knobs, so to ensure that the two would move in unison, we applied tacky electrical tape to the inside of the ring, greatly increasing friction and allowing the mount knobs to be turned with the rotation of the motors.

Figure 4, Adjustment Knob Mount

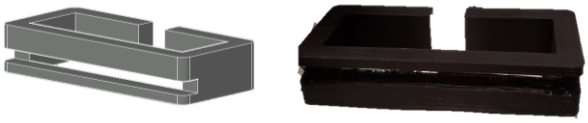

Figure 5, Adjust Motor Housing

Unless the knob motors themselves are anchored in a fashion that restricts their movement, rotation of the motors would simply rotate the motor housings rather than the adjustment knobs. To circumnavigate this issue, a motor casing was designed to house both motors to keep their position static as they applied torque to the adjustment knobs. Other considerations had to be accounted for when designing this casing, as it would need to have a negative space clearing in order to allow the beam of the laser to pass through unobstructed. Furthermore, the wires of the motors had to retain their connection to the adjustment systems PCB, explaining the small slit on one edge of the casing. Also important was the fact that the casing could not be hard fastened to the optic mount itself as the stand motor would rotate and alter the casing's position.

As well as this, a mechanism for rotation of the couplers post had to be designed, since the positional servo motor could not be easily located underneath or above the

couplers mount in order to rotate it about the axis of the optical post. The rotation of the positional motor was simply translated linearly to the location of the stand post via two arms and a spacer for the post to allow the stand to be rotated at a distance by the motor. The two elements below with holes on either end are the arms, whereas the piece with the circular ring extrusion wraps around the coupler's optical post. This piece also has a hole bored into its side, to allow for a screw to be threaded through it and ensure maximum friction between the coupler post and the part. On the other side of the arms lies the piece which connects to the servo motor. This connection was created by etching an imprint of the servo motors propellor into the bottom of the piece and recessing it deep enough to allow it to fit snugly over the propellor.

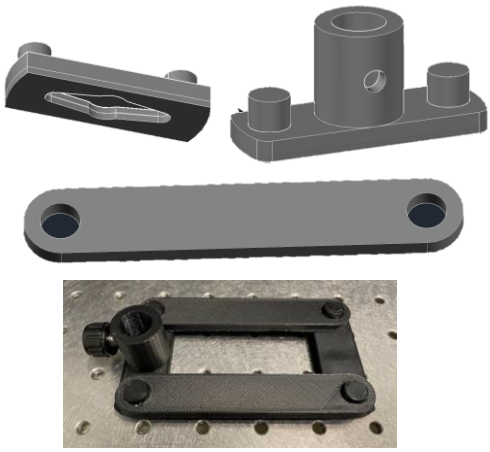

Figure 6, Coupler Servo-Motor Interface

The final parts our group had to develop and design were a mounting table for our optical elements and a housing for the positional servo motor. Early in the development of these parts, we decided to connect the two so we could reduce the number of optical posts used in setting up the system. By doing this, the total number of posts in set-up is 3, with only one of those posts being needed for our parts (1 post for the laser, 1 for the coupler, and 1 for the optics table). The design of these elements was relatively simple; the main concern was ensuring that our optics and the servo motor's center of rotation would be aligned along the same axis as the beam. Surprisingly, the servo motors center was skewed toward the side, requiring us to slightly redraft our design for the servo cage on multiple occasions. Another consideration in the design was making it so that the required spacing between this unit and the coupler was easily identifiable, thus we purposely spaced the elements so that the distance between the optical posts of the cage-mount unit and the optical post of the coupler unit are spaced 6 bore holes apart on a standard optical breadboard, roughly 6 inches.

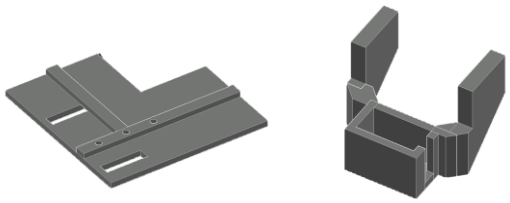

Figure 7, Optical Track and Stand Motor Housing

E. Optics

For all the optics discussed below, 3-D printed casings were designed which could cleanly fit on the ridges present in the optics mount discussed above. The design of these was trivial and did not warrant further discussion.

We chose a plate beam-splitter for their lower costs, at least in comparison to cube beam splitters. Plate splitters are also smaller and lighter than most cube splitters, an important consideration to meet our weight and size specifications. This choice of plate splitter came with the unfortunate downside of lateral displacement of the beam as it travels down the optical axis. This negative consequence is mitigated by the focusing lens, discussed in the next section.

Ideally, the active area of the power meter photodiode would be rather large, to be able to capture laser light from a relatively wide range of incident angles and lateral displacements. However, photodiode active areas are produced from high quality semiconductor material that are expensive in large quantities. Thus, it was the more affordable option to purchase a photodiode with a smaller active area and utilize a focusing lens to bring displaced laser light to be incident on the photodiode. A simple, low-cost, 12.7mm diameter, 50.0mm focal length, N-BK7 biconvex lens was the best option. This optic essentially increases the active area of our photodiode without needing to by a larger photodiode. Through varying the lateral position of the laser via a linear translation stage, it was found that the focusing optic increases our horizontal range of detectable beam locations by about 3.1 times. The beam profiler makes use of the focusing lens to determine the beams angular divergence as well.

The neutral density (ND) filters included in this project are utilized in a toggled fashion. If the laser being used is too low power, then the presence of the ND filters may

make the incoming signal too weak. Conversely if the laser is too powerful, then the lack of ND filters could damage the camera sensor and photodiode. The user will have to determine whether the filters should be employed on a case-by-case basis.

F. PCB Design

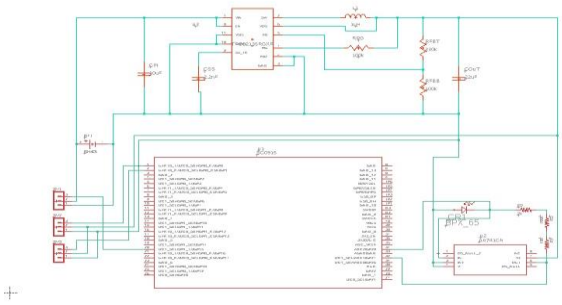

Figure 7, PCB Schematic

For this project, designing of the PCB board was done on Autodesk Eagle software. As seen in figure 7, the power meter and the mirror mount motors were relocated to each side of the Raspberry Pi Pico with the mirror mount motors dealing with pins 1-20 while the power meter is connected to various pins between pins 23-38. Though the PCB contains the power meter and the motor system, initially the plan for the PCB was to include much more such as the power supply and multiple voltage converters. However, over the course of the project the PCB design drop the mentioned components for several reasons. For the voltage converter the main reason as to why it was dropped was due to supply shortages. When designing the voltage converter, the website Webench was used, but for each design the same issue occurred where key components were out of stock, eventually making a DC converter unfeasible with the projects time restraints. As a result of this, a prebuilt DC converter was bought instead. For the voltage supply, a BHDL4xD battery pack was used, however, having a whole area on the PCB for the battery pack proved unnecessary. Its spot aboard the PCB was replaced with pin holes connected to the ground and voltage inputs of all the major components. As a result of the constant changes, additional pin holes were placed in the PCB board, mainly for ground voltage inputs and voltage outputs. These acted as redundancies in the PCB design, in case of any more problems arising while developing the project.

G. Laser Alignment Software

Our original plan to achieve alignment of the laser was to utilize a Q-Learning based reinforcement learning algorithm to both align the laser and reach maximum power. This initial approach had a few shortcomings which we hadn't foreseen in our initial planning stages. Any differences in the set-up of the physical components of the system would result in any data from previous alignments being useless. As a result, we adapted our approach to utilize a threshold search algorithm. The threshold search algorithm works by scanning vertically with the mirror while sweeping back and forth horizontally until a flash of lasing is detected on the power meter. Once the vertical orientation is located the system begins adjusting the mirror horizontally in small increments until a large jump in intensity is detected by the power meter. This approach proved very effective in aligning the laser as the range of positions that allowed for alignment were large in comparison to the movements we were able to make using the continuous motors. Our approach for finding the max power of the laser was to first run the alignment algorithm for initial lasing. From that point we would scan vertically until the laser went from lasing to not lasing and find the point which resulted in the highest power. We would then return to that orientation and then scan horizontally once again looking for the max power until the laser reached the boarder of the lasing threshold and returning once again to the max power orientation. This approach did result in finding a higher power than the initial alignment, but since the continuous motors moved at different speeds when moving forward and backward it was inconsistent when trying to return to the exact location of max power.

III. CONCLUSION

The product fulfilled each of the primary goals outlined for the project – taking the laser from not lasing to lasing, finding the maximum laser power, and provide beam diagnostics and feed to the user via a beam profiler. During the development cycle of this project, each member of our team had to apply themselves to an engineering challenge beyond the scope of their academic training. Whether that be an optics student 3-D modeling mechanical elements or a computer science major analyzing focusing lenses, we each broadened our engineering skillset. Furthermore, we gained priceless experience in working in a multidisciplinary team towards a shared goal and developed our abilities at interpersonal communication.

References

A., Saleh Bahaa E, and Malvin Carl Teich. Fundamentals of Photonics. John Wiley & Sons, Incorporated, 2019.

Dereniak, Eustace L., and Teresa D. Dereniak. Geometrical and Trigonometric Optics. Cambridge University Press, 2008.

Kammet, Joel. Exploring Robotics Supplemental Notes . https://www.sci.brooklyn.cuny.edu/~kammet/gear_notes.pdf.

Paschotta, Dr. Rüdiger. "RP Photonics Encyclopedia." RP Photonics , 26 Sept. 2021, https://www.rp-photonics.com/index.html.

Sutton, Richard S., et al. Reinforcement Learning: An Introduction. MIT Press Ltd, 2018.

Acknowledgments

Our group would like to thank every professor who has helped us along our academic journey in anyway. We have special thanks for Dr. LiKamWa and Ph.D. candidate Dmitrii Konnov, who graciously lent us an open cavity laser to use in the development and testing of our project. Without them, we never could have done this.

About the Authors

William Matthew Bowman
Matt is in his fourth year at the University of Central Florida and will receive his Bachelor's of Science in Photonic Sciences and Engineering in 2022. He is currently working as a research assistant for Dr. Luca Argenti. His interests lie in photovoltaic cells for solar energy and nanophotonics.

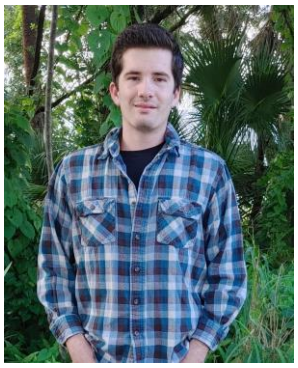

Bryce Moon
Bryce is in his fifth year at the University of Central Florida. He plans on graduating with a bachelor's degree in Electrical Engineering, specializing in power and renewable energy. After graduation, Bryce plans to enter the work force, ideally under the employment of Duke Energy, FPL or another power distribution company.

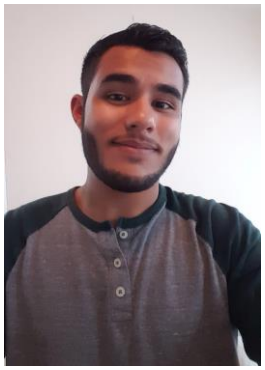

Anthony DeSantis
Anthony is in his fifth year at the University of Central Florida. He will be graduating with a bachelor's degree in Computer Engineering. After graduating he will be working for Northrop Grumman Corporation as a Software Engineer.

Nicholas Pinkham
Nicholas is in his fifth year at the University of Central Florida, planning to graduate in Optics. Next Autumn, he will begin a master's program in Computational Color and Spectral Imaging through the European Erasmus Program. At UCF, Nicholas does research under Dr. Eikenberry designing integrated optics for telescope arrays.